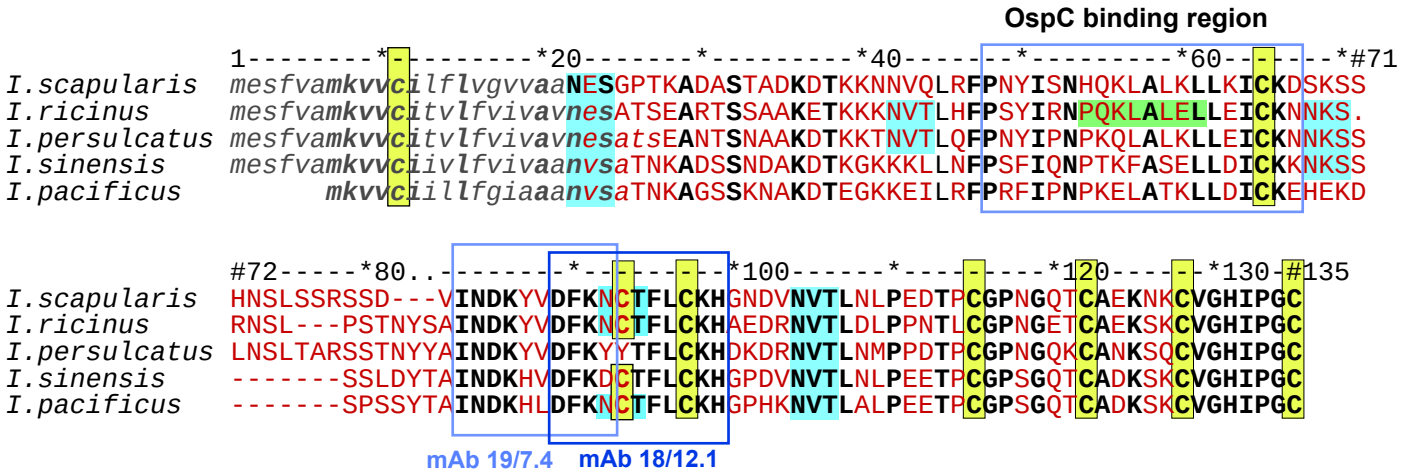

Fig. S1. Alignment of Salp15 orthologs from various *Ixodes* species. The alignment was generated using COBALT as implemented in the NCBI suite. Genbank accession codes for the Salp15 orthologs are: *I. scapularis*, AAK97817; *I. ricinus*, ABU93613; *I. persulcatus*, ACV32167; *I. sinensis*, AFV41216; *I. pacificus*, ACV32166. Signal sequences predicted by SignalP 4.1 (www.cbs.dtu.dk/services/SignalP/) are shown in grey lower case lettering, absolutely conserved residues in bold black or grey (signal sequences), variable residues in red; chemical similarity between variable residues was not considered. Numbering refers to Salp15 from *I. scapularis*. N-Glycosylation motifs are highlighted by light blue background, cysteines by yellow boxes, and the experimentally proven α-helix in Iric-1 by green background. Note the very high conservation of the region containing the mAb 18/12.1 and 19/7.4 epitopes, and the conserved pattern of hydrophobic and charged residues in the C terminal part of the OspC binding region.

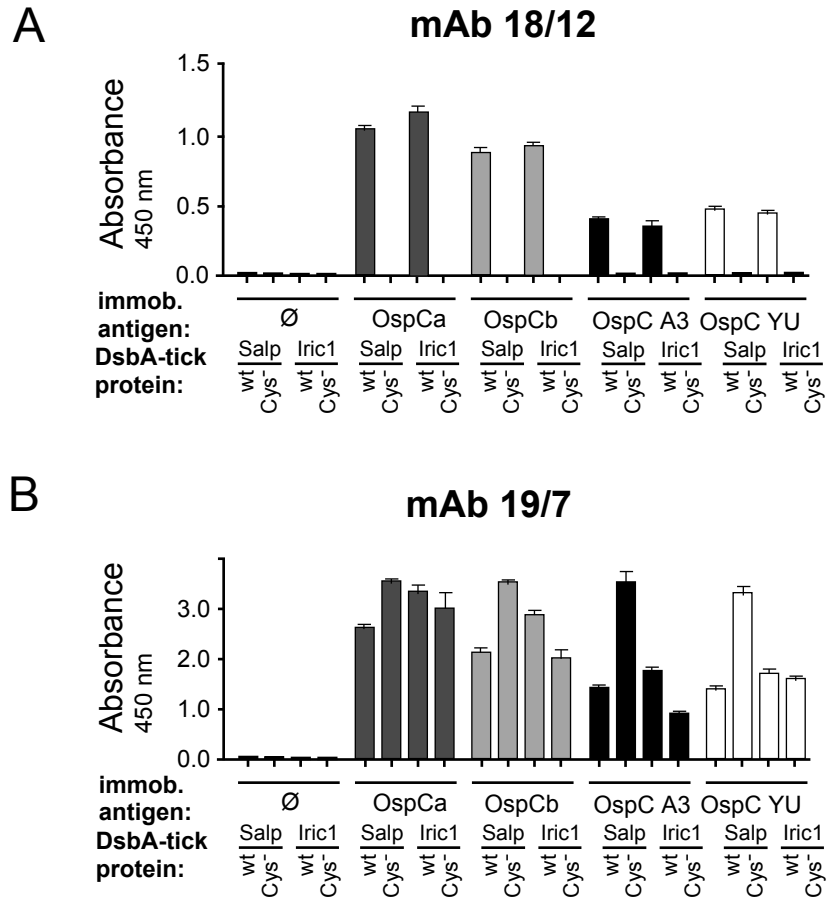

Fig. S2. Mapping of the OspC interaction sites on Salp15 and Iric-1 using a mAb 18/12.1-based OspC binding ELISA. ELISA plate wells were coated with recombinant OspCa as in Fig. 8, then incubated, or not (ø), with the indicated DsbA-fused deletion variants of Salp15 or Iric-1. Bound tick proteins were detected using mAb 18/12.1 (A). For convenience, the analogous assay performed with mAb 19/7.4 (Fig. 8) is shown again in (B). The lack of signals of the assays involving the Cys-free variants of Salp15 and Iric-1 with mAb 18/12.1 confirms in a non-denaturing setting the cysteine-dependent nature of the mAb 18/12.1 epitope. For the wild-type tick proteins, the higher signals with the two *B. burgdorferi* (OspCa, OspCb) versus *B. afzelii* OspC proteins (OspC A3, OspC YU) with mAb 18/12.1 are congruent with the mAb 19/7.4 results.

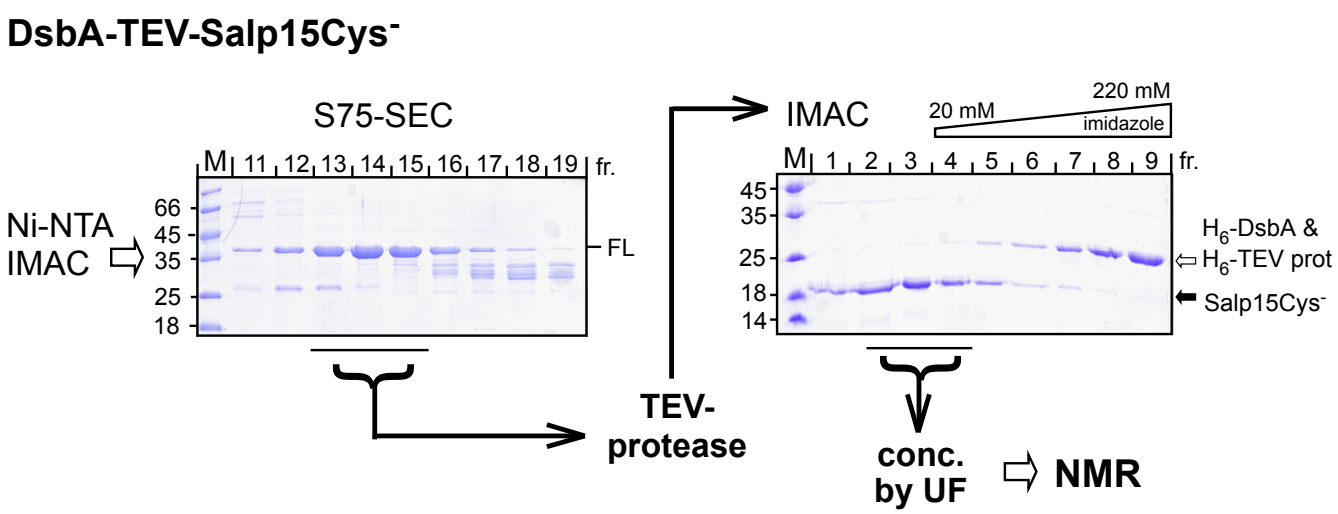

Fig. S3. Purification of free Cys-less ^{15}N-Salp15 for NMR. The DsbA-TEV-Cys--Salp15 fusion protein was expressed in SHexpCP cells grown in ^{15}NH4Cl-supplemented minimal medium and enriched via Ni^{2+} IMAC using the N terminal His6-tag on DsbA as shown in Fig. 3A for the wild-type Salp15 DsbA fusion protein. The peak fractions were subjected to SEC on Superdex 75 (*left panel*) to remove the bulk of truncated products. The peak SEC fractions containing the full-length (FL) protein were subsequently incubated with His-tagged TEV protease (as in Fig. 9), and free Cys-less Salp15 was separated from the His-tag containing uncleaved precursor, DsbA and TEV protease *via* inverse IMAC. The flow-through was concentrated *via* ultrafiltration (UF) and the concentrate was used for NMR.

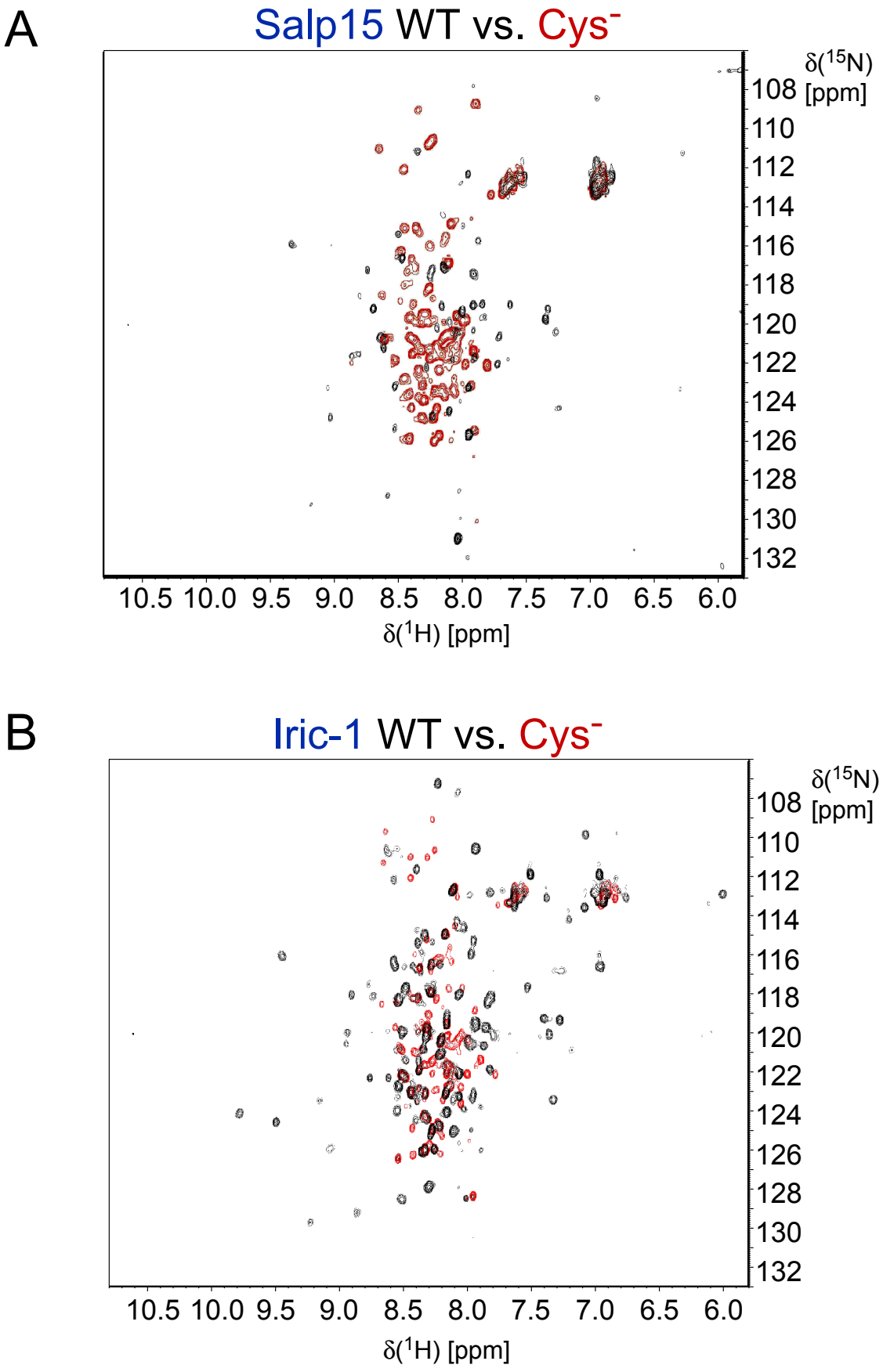

Fig. S4. 1H-15N HSQC NMR spectra of protease-released wild-type versus Cys-free Salp15 and Iric-1. (A) Salp15. (B). Iric-1. The spectra are enlarged versions of those shown in Fig. 10D and 10E.

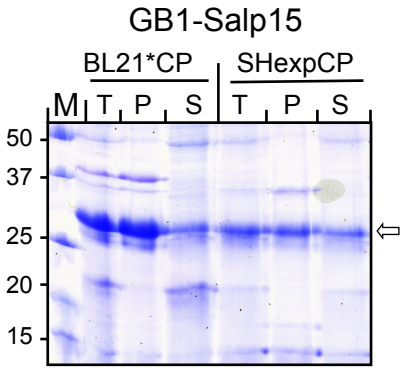

Fig. S5. Comparison of GB1-Salp15 expression in BL21*CP versus SHexpCP cells. GB1-Salp15 was expressed in either BL21*CP or SHexpCP cells. After cell lysis under native conditions, equal aliquots of the total protein (T) before centrifugation, and in the insoluble pellet (P) or soluble supernatant (S) after centrifugation were analyzed by SDS-PAGE. As for the DsbA fusion proteins (Fig. 2C), the total amounts of fusion protein expressed were higher in BL21*CP cells, yet the amounts of soluble protein were comparable in SHexpCP cells and contained fewer truncated products. However, compared to the DsbA fusions (Fig. 2C), substantially more of the GB1-fusion protein remained in the insoluble fraction, attesting to the superior solubility enhancement by DsbA.

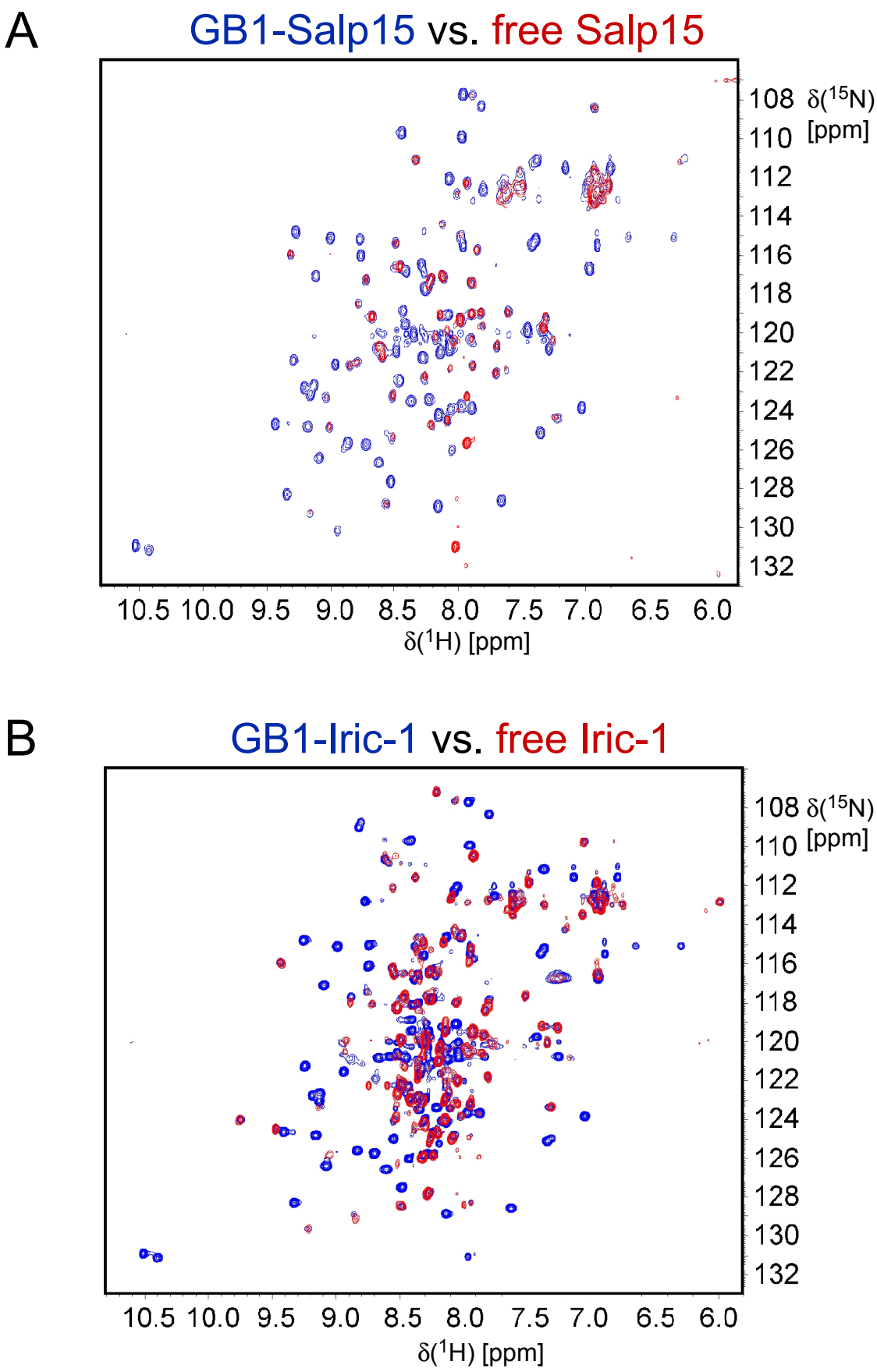

Fig. S6. ^{1}H-^{15}N HSQC NMR spectra of GB1-fused versus free Salp15 and Iric-1. (A) Salp15. (B). Iric-1. The spectra are enlarged versions of those shown in Fig. 11A and 11B.

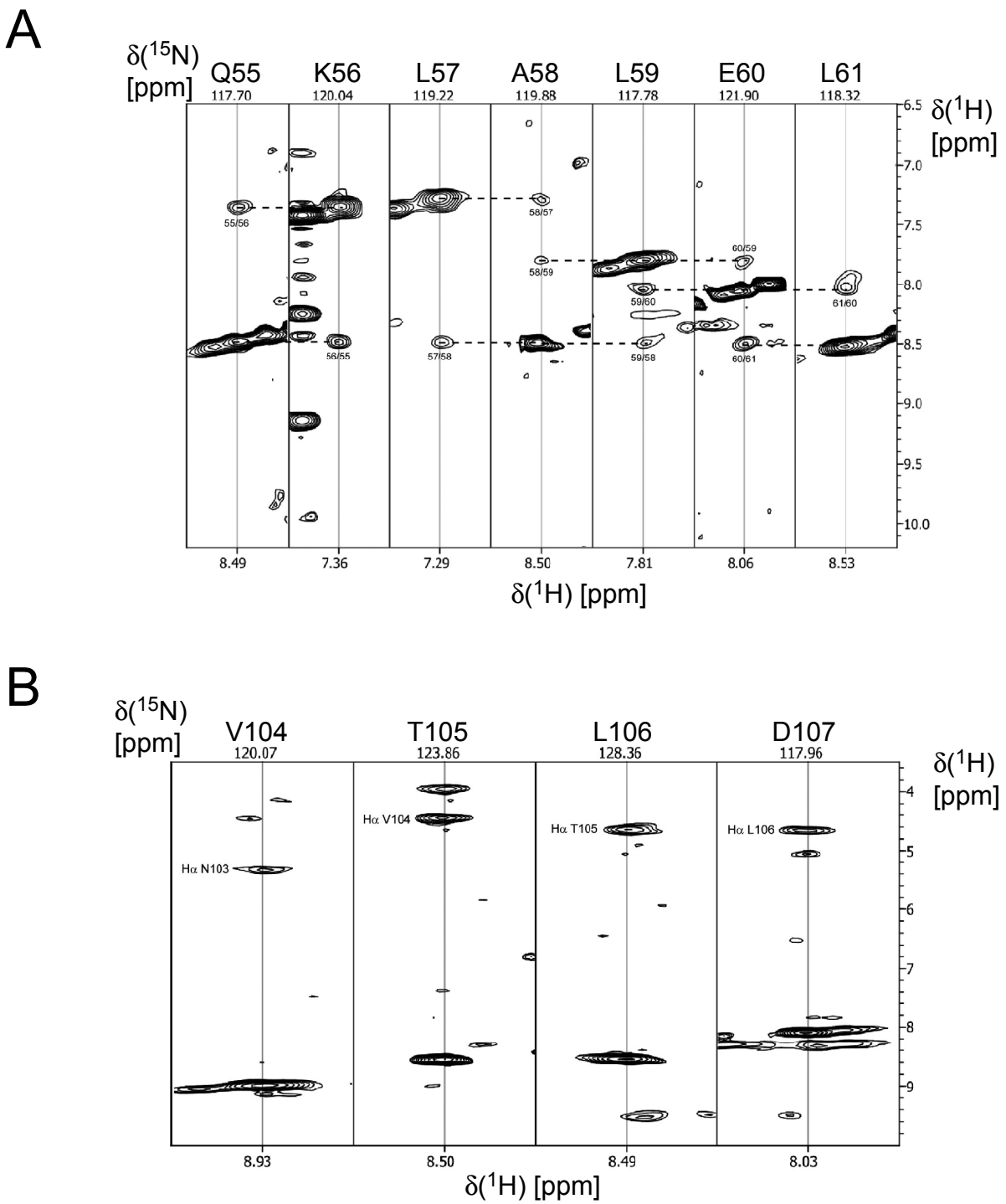

Fig. S7. Experimental evidence for secondary structure elements in the Iric-1 part of GB1-Iric-1 from NOESY-1H-15N-HSQC spectra with 100 ms mixing time. Strip plots of the relevant regions are shown. **(A) Iric-1 residues Q55 - L61 form an α-helix.** The plot shows the characteristic sequential NH-NH cross peaks that identify the α-helical conformation. **(B) Iric-1 residues V104-D107 are involved in a β-strand.** The plot shows strong sequential Hα-NH cross peaks characteristic of a β-strand and the typical downfield shift of the Hα protons. For a schematic overview see the TALOS-N plot in Fig. 11C.